REALIZATION OF HIGH-INTENSITY BEAMS WITH SMALLER EMITTANCE WITHOUT A TRANSVERSE FEEDBACK SYSTEM

Y. Shobuda*†, P. Saha, Japan Proton Accelerator Research Complex, Tōkai Mura, Japan
T. Toyama, High Energy Accelerator Research Organization, Tsukuba, Japan
I. Yamada, Japan Atomic Energy Agency, Tōkai Mura, Japan
N. Yoshimura, Toshiba, Kanagawa, JAPAN

Abstract

The RCS at J-PARC is a kicker-impedance-dominant machine, which exceeds the impedance budget from a classical viewpoint. However, we have achieved a 1-MW beam without any transverse feedback by fully utilizing the indirect space charge effect (due to chamber walls) to suppress beam instabilities. Although the indirect space charge effect is beneficial, the beam instability can still occur in a high-intensity beam with a smaller transverse emittance. To address this, we installed diode stacks and resistors at the ends of the four kicker power cables and have successfully conducted routine operations. This approach theoretically opens the door to achieving high-quality, higher-intensity beams, including a 2-MW beam, as no transverse feedback is required.

INTRODUCTION

The 3-GeV RCS [1] at J-PARC [2] is a proton accelerator to achieve a one megawatt beam by accelerating two bunches containing $N_b = 4.15 \times 10^{13}$ particles per bunch from 400 MeV to 3 GeV in 20 ms with a repetition rate of 25 Hz [3], without any transverse feedback system.

The RCS provides proton beams downstream to both the Material and Life Science Facilities (MLF) and the Main Ring (MR) by accumulating the injection beams from LINAC, following a painting scheme [4]. The standard unnormalized transverse painting emittance, the unnormalized value of the entire painting area, for the MLF is relatively large (e.g., 200 π mm-mrad). However, the smaller emittance would be better (typically ~ 50 π mm-mrad) for the MR, because the beams extracted from the RCS are delivered to the MR through the beam extraction line with a small mechanical aperture, exciting a large residual dose.

In the case of a smaller-emittance beam, special care must be taken regarding space-charge effects. This is because the smaller emittance beam increases the tune spread, expanding the probability of resonance crossing of particles, which restricts the available operational tune on the tune diagram because of the beam losses.

On the other hand, the beam coupling impedances [5] can drive the beam instabilities [5], which may be mitigated by selecting the other tunes.

However, both desirable tune regions for avoiding the resonance crossing and for suppressing the beam instabilities may compete with each other, thereby limiting the overall tunability of machine operation, urging the reduction of the impedance causing the beam instability.

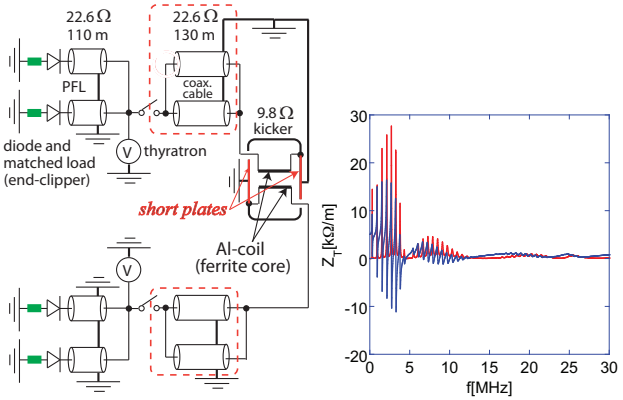

Figure 1: kicker (left); horizontal impedance Z_T (right) with the real part in red and the imaginary part in blue [8].

BEAM-INSTABILITIES AT THE RCS

Historically, the 3-GeV RCS at J-PARC was designed below the impedance budget, except for the kicker impedance from a classical viewpoint [6]. The horizontal impedance $Z_T(\omega)$ at Lorentz-$\beta_s = 1$ for one kicker is shown in the right panel of Fig. 1. Eight kickers (specified by Kicker Nos.1-8) whose impedance is around ten times higher than SNS kicker impedance [7] were installed into the RCS.

The enhancement of the kicker impedance is closely related to the merit of the power-saving of the kicker magnet. As shown in the left panel of Fig. 1, the kicker at the RCS is a transmission line type embedding two ferrite cores. The kicker has four terminals: two connected to the power supply through 130-m-long coaxial cables, and the other two terminated in a short circuit [9]. Shorting the kicker terminals benefits beam extractions by doubling the excitation currents, leading to power savings. Meanwhile, the impedance is enhanced during the acceleration period because the beam-induced current created by the beam passing through the kicker coil is accumulated and retained on the kicker cable owing to the absence of any resistors [10].

Because of the spike structure of the impedance shown in Fig. 1 originating from the kicker cable with open terminal, the beam growth rate critically depends on the operational tune [8]. The left panel of Fig. 2 shows the measured horizontal beam positions for a beam with $N_b = 3.15 \times 10^{13}$ particles per bunch (0.76-MW beam), color-coded according to the tune tracking during the acceleration in the right

* yoshihiro.shobuda@j-parc.jp

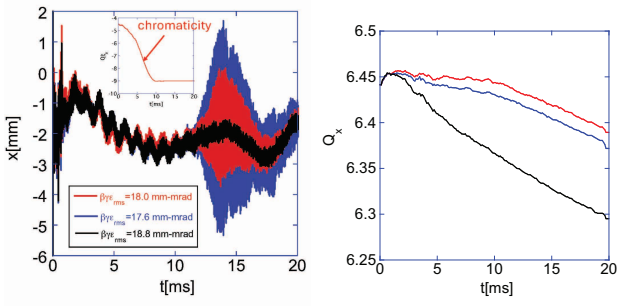

Figure 2: Dependence of beam positions (left) on tune tracking patterns (right) for a 0.76-MW beam.

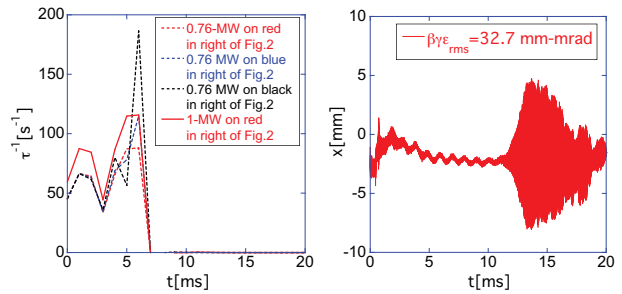

Figure 3: The beam growth rates by the conventional theory (left) and the measured beam positions for a 1-MW beam (right) under the red tracking pattern in the right of Fig.2.

panel, where the sextupole magnet initially corrects half of the chromaticity at the injection energy but is turned off at 10 ms [11]. The beam becomes unstable for the red and blue patterns, while it is stable for the black one.

Despite the kicker impedance exciting beam instability [12], the underlying mechanism remains mysterious. This is evident because the beam growth rates for 0.76-MW and 1-MW beams, estimated by the conventional Sacherer's formula [13]—which neglects space charge effects—significantly differ from the measured values. Specifically, the predicted rates (solid and dashed lines in the left panel of Fig. 3) contrast sharply with the measurements shown in the left panel of Fig. 2 (for 0.76-MW) and the right panel of Fig. 3 (for 1-MW). The color-coding used in the left panel of Fig. 3 corresponds to the tune tracking displayed in the right panel of Fig. 2. Notably, the instability is observed

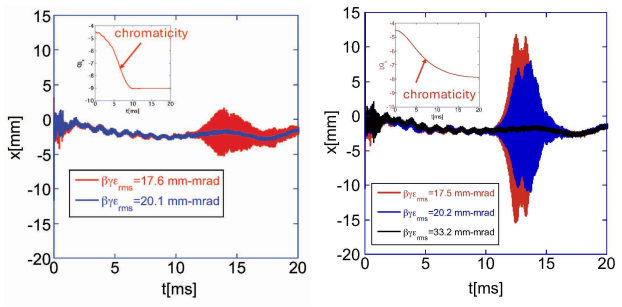

Figure 4: Dependence on chromaticity and emittance for a 0.76-MW beam under the blue tracking in the right of Fig.2.

at higher energies, contrary to theoretical expectations, even when the sextupole magnet is turned off at 10 ms, for both the 0.76-MW and 1-MW beams.

Figure 4 shows the measurements for a 0.76-MW beam with different measured transverse emittance [14] on the blue line in the right of Fig. 2 under different sextupole conditions : (left) when the sextupole magnet initially corrects half of the chromaticity at the injection energy but is turned off at 10 ms and (right) when the sextupole magnet corrects half of the chromaticity at the injection energy using a DC power supply. As a result, we can confirm that the increase in chromaticity in the negative direction suppresses the beam growth rate in the machines with a negative slippage factor, like the RCS [1].

Figure 4 reveals an emittance dependence on the beam growth rate, regardless of the choice of chromaticity. Furthermore, the previous study [8] shows that the beam is not always stabilized for beams with lower peak currents, or larger bunching factor : B_f (the average current divided by the peak current). These results suggest that the space charge significantly affects the beam growth rate.

In the next section, we will illustrate a theory dealing with the space charge effects on the beam instabilities.

SPACE CHARGE EFFECTS ON THE BEAM INSTABILITIES

The beam growth rate, including the space charge effect, is given by the real part of $j\omega_0\nu$ by solving the following dispersion relation for ν as a function of nominal betatron tune Q_x [8]:

$$\sum_{p=-\infty}^{\infty} \frac{je^2 N_b M \beta_s^2 \sum_{i=1}^{N_{kicker}} \beta_x^{(i)} Z_T^{(i)} \left(\omega_0(\Re[\nu] + \mu + pM)\right)}{8\pi^2 J_{x0} p_s R \left(m\frac{d\nu_L}{dJ_x} + \frac{d\nu_x}{dJ_x}\right)}$$

$$\times \left| J_m \left[\left(\nu + \mu + pM - \frac{Q_x \xi_x}{\eta} \right) \sqrt{\frac{2\omega_0 J_{L0}|\eta|}{c p_s \beta_s \nu_{s0}}} \right] \right|^2$$

$$\simeq -\frac{1}{\left[1 + \frac{(\nu - m\nu_{L0} - \nu_{X0}) e^{-\frac{(\nu - m\nu_{L0} - \nu_{X0})}{\left(m\frac{d\nu_L}{dJ_x} + \frac{d\nu_x}{dJ_x}\right) J_{x0}}} \Gamma\left[0, -\frac{(\nu - m\nu_{L0} - \nu_{X0})}{\left(m\frac{d\nu_L}{dJ_x} + \frac{d\nu_x}{dJ_x}\right) J_{x0}}\right]}{\left(m\frac{d\nu_L}{dJ_x} + \frac{d\nu_x}{dJ_x}\right) J_{x0}} \right]}, \quad (1)$$

where

$$m\frac{d\nu_L}{dJ_x} + \frac{d\nu_x}{dJ_x} \simeq m \left. \frac{dY'_{coh,2}(J_L)}{dJ_L} \right|_{J_L = J_{L0}} \frac{\langle \beta_x(s) \rangle}{p_s} + 3 \left\langle \beta_x^2(s) \right\rangle Y'_{coh,4}(J_{L0}), \quad (2)$$

$$\sigma_x = \sqrt{\langle \beta_x(s) \rangle \epsilon_{x,rms} + \langle D^2(s) \rangle \left(\frac{\Delta p}{p}\right)^2}, \quad (3)$$

$$J_{x0} = \frac{\beta_s E_s \epsilon_{x,rms}}{c}, \tag{4}$$

$$\nu_{L0} = \nu_{s0} + \left.\frac{dY'_{coh,0}(J_L)}{dJ_L}\right|_{J_L=J_{L0}}, \tag{5}$$

$$\nu_{X0} = Q_x + \frac{\langle \beta_x(s) \rangle}{p_s} Y'_{coh,2}(J_{L0}), \tag{6}$$

$$\sigma_z = \frac{c}{\omega_0}\sqrt{\frac{2J_{L0}|\eta|\omega_0}{E_s \nu_{s0}}}, \tag{7}$$

j is imaginary unit; N_{kicker} is the number of kicker; $\beta_x^{(i)}$ is the β-function at which i-th kicker is located; $Z_T^{(i)}$ is i-th kicker impedance; m and μ are the head-tail and coupled modes, respectively; ω_0 is angular revolution frequency; h is harmonic number; c is light velocity; $E_s = cp_s/\beta_s$; p_s is the longitudinal momentum of the synchronous particle; β_s and γ_s are the Lorentz-β and the Lorentz-γ of the particle; η is slippage factor; ξQ_x is chromaticity in the horizontal direction; Z_0 is impedance of free space; $J_n(x)$ is the Bessel function; $\Gamma[0,z]$ is the incomplete Γ-function; M is the number of bunches (buckets); $\epsilon_{x,rms}$ is the root mean square (rms) emittance of the beam; $\Delta p/p$ is the momentum spread; J_{L0} is the longitudinal beam emittance; ν_{s0} is the nominal synchrotron tune; ν_{L0} and ν_{X0} are the coherent synchrotron and betatron tunes; $\beta(s)$ and $D(s)$ are the β- and dispersion functions, respectively; R is the average radius of the RCS; and $\langle\cdots\rangle$ denotes the average value around the ring. The functions $Y'_{coh,0}(J_L)$, $Y'_{coh,2}(J_L)$ and $Y'_{coh,4}(J_L)$ are derived in the reference [8]. Here, the original formula in the reference [8] is extended to include the $\beta_x^{(i)}$ dependence for the i-th kicker.

The left panel of Fig. 5 shows the B_f-dependence of the beam growth rate at 15 ms with $Q_x = 6.45$, where the chamber radius a is assumed to be 145 mm and ξQ_x is fully corrected at the injection energy using a DC power supply, corresponding to the measurement in [8]. The beam growth rate critically depends on B_f. Furthermore, the beam growth rate becomes higher as B_f gets larger around the regions A and B. Increasing the peak current can stabilize the beam, contrary to the conventional understanding, due to the space charge effect, explaining the measurements.

The right panel of Fig. 5 shows the tune dependence of the beam growth rate from 13 through 15 ms for a 0.76-MW beam, corresponding to Fig. 2. We can understand that the kicker impedance described in Fig. 1 causes the beam instability with the operation tune crossing around 6.4-6.45.

Figure 6 shows the normalized $\epsilon_{x,rms}$-dependence of the beam growth rate at 14 ms for the chamber radius: $a = 145$ mm and $a = 160$ mm in both cases: (left) when the sextupole magnet initially corrects half of the chromaticity at the injection energy but is turned off at 10 ms, and (right) when the sextupole magnet corrects half of the chromaticity at the injection energy using a DC power supply. The direct space charge effects (repulsive forces in an open boundary) remain constant, whereas the indirect space charge effects, originating from the ideal, perfectly conductive chamber boundary, vary with the chamber radius.

The increase in chromaticity suppresses the beam growth rate in Fig. 6, consistent with the measurements in Fig.4. Moreover, the beam instability is suppressed around 20 mm-mrad for $a = 145$ mm in the left panel, explaining why the blue line is suppressed in the left panel of Fig. 4. Here, it is essential that the beam has a finite transverse size relative to the chamber radius a, from the perspective of beam instability, because the damping effect is activated by indirect space charge effects, leading to the suppression of beam instability at low energy. Simulations have established the indirect space charge damping effect by observing the chamber radius dependence of beam growth rate [15].

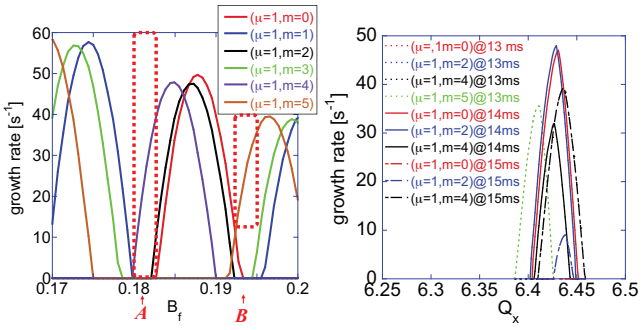

Figure 5: Bunching factor- (left) and tune- (right) dependences of the beam growth rate with $\beta_s\gamma_s\epsilon_{x,rms} \simeq 17.6$ mm-mrad for a 0.76-MW beam, where $a = 145$ mm.

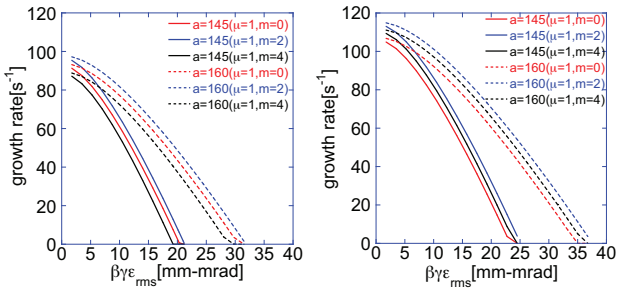

Figure 6: Emittance-dependence of the beam growth rate for a 0.76-MW beam at 14 ms, corresponding to Fig.4, in the cases of $a = 145$ mm (solid) and $a = 160$ mm (dashed).

We have demonstrated the space charge damping effects by realizing 1-MW beams in the RCS. However, it remains under discussion whether the space charge effects actually damp the instabilities, since a theoretical model that neglects indirect space charge predicts stronger instabilities than in the case where only wake fields are considered [16]. If this theoretical prediction holds, the kicker impedance specific to the RCS may incidentally stabilize the beam.

Recently, Yoshimura, Toyama, and Shobuda [17] have resolved this discrepancy by investigating the space charge effect in the MR with the resistive-wall impedance under the 3-GeV storage mode. Their simulations deal with a two-dimensional (longitudinal+horizontal) model, with a linear approximation applied to the space charge. Nonetheless, the

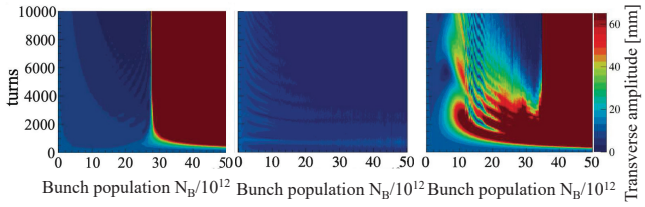

Figure 7: Amplitude along the turn number (vertical) for the respective bunch populations (horizontal) [17].

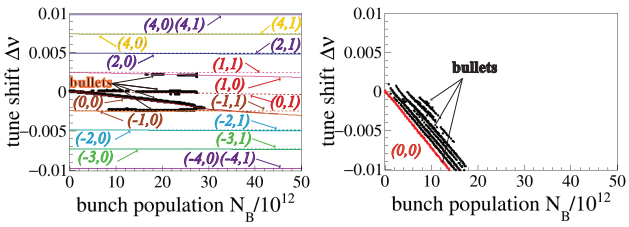

Figure 8: Tune shift specified by (head-tail mode, radial mode) without (left) and with space charge (right) [17].

approximation is justified when the transverse beam size is significantly smaller than the chamber radius [17].

Figure 7 illustrates the oscillation amplitude of the bunch along the turn number for the respective bunch populations under three different conditions, where the chromaticity is fully corrected with only the resistive-wall impedance included (left), the impedance as well as the space charge effects considered (center), and only the indirect space charge effects neglected (right). The space charge damping effect is obvious because the beam growth rate is most reduced when all space charge effects are taken into account (center). Moreover, the beam growth rate is most enhanced when only the indirect space charge is neglected (right), which is consistent with the theoretical prediction accounting for only the direct space charge effect with wake forces.

More specifically, the bullets (••···) in Fig. 8 show the tune shifts obtained from the simulations. The left panel, which includes only the resistive-wall impedance, agrees with the conventional theoretical results denoted by the solid and dashed lines, labeled by (head-tail mode, radial mode) and obtained using the Vlasov solver [18, 19], where the transverse mode-coupling instability (TMCI) is identified. In contrast, the right panel shows that the space-charge effect suppresses the negative head-tail and radial modes, resulting in the excitation of only positive head-tail modes with the lowest radial mode. This is the mechanism responsible for the mitigation of TMCI due to space-charge effects.

Though the theory describing the RCS suggests that the nonlinear effect due to the indirect space charge seems to be crucial for the damping effect, the new research reveals that the linear component of the indirect space charge is essential to suppress the beam instability. Moreover, the feature of the kicker impedance at the RCS is not critical in suppressing the beam instability, because we find that the beam instability can be suppressed by activating the indirect

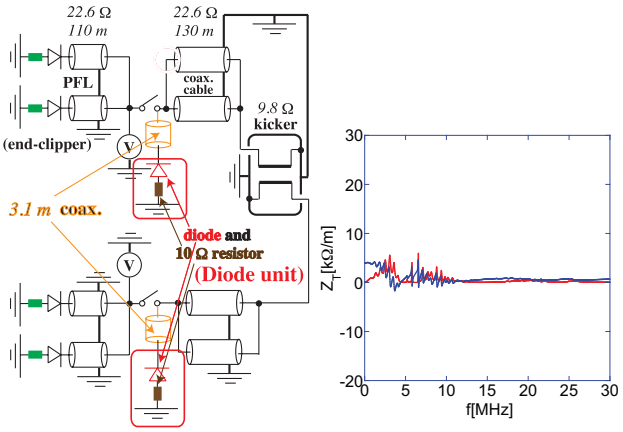

Figure 9: Modified kicker (left) [11] and horizontal impedance Z_T (right) with real part in red and imaginary part in blue.

space charge damping effect for the more general case of impedance, i.e., the resistive-wall impedance [20].

Since the beam size relative to the chamber radius is crucial to suppress the beam instability, modifying the kicker with the benefits of shorted kicker ends retained is inevitable for the future higher power operations with small emittance beams for the MR [21].

KICKER IMPEDANCE SUPPRESSION

To suppress the kicker impedance, we developed a diode stack with matched resistors (diode unit) and inserted it at the end of the kicker terminals, preceding the thyratron switch, as illustrated in the left panel of Fig. 9 [11, 22]. This scheme doubles excitation currents with shorted ends by preventing the forward current from the Pulse Forming Line (PFL) from flowing into the matched resistors [23].

Meanwhile, high-frequency beam-induced currents pass through the diodes and are absorbed by the matched resistors, effectively suppressing the kicker impedance, as shown in the right panel of Fig. 9, which presents the impedance at $\beta_s = 1$ for a 1-MW beam. This suppression occurs because the diode forms an insulating depletion layer between the anode and cathode under reverse bias. As a result, the diodes act as both capacitors and rectifiers, reducing the impedance.

Since November 2024, four pairs of diode units have been installed into four out of eight kickers, with the RCS delivering high-intensity beams under routine operation.

BEAM INSTABILITY SUPPRESSION

Now, we investigate how the beam growth rate is suppressed by modifying the terminal conditions of the kicker cables both theoretically and through measurements.

Figure 10 shows the horizontal beam positions for a 0.76-MW beam with around 18 mm-mrad rms normalized emittance, color-coded according to the tune tracking in the right panel of Fig. 2, where the sextupole magnet initially corrects half of the chromaticity at the injection energy, but is turned off at 10 ms. In the left, center, and right panels, the diode

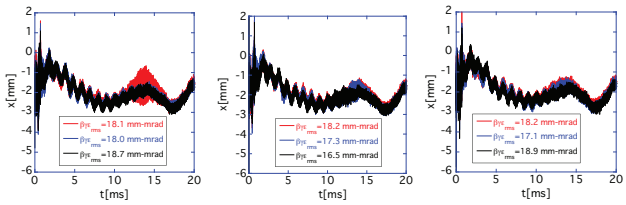

Figure 10: Dependence on tune tracking patterns with diode units attaching only to No. 8 (left), only to No. 5 (center), and to both Nos. 5 and 8 (right) for a 0.76-MW beam.

units are attached only to Kicker No. 8, only to Kicker No. 5, and to both Kickers Nos. 5 and 8, respectively. Compared to the results in Fig. 2, the diode unit suppresses the beam instability for this small emittance beam. Moreover, there appears to be a kicker position dependence for the effectiveness of the damping effect, as the reduction of the beam growth rate is activated through the beta function at which the kickers are positioned in the RCS ($\beta_x^{(5)} = 18.1$ m, and $\beta_x^{(8)} = 10.4$ m) [15].

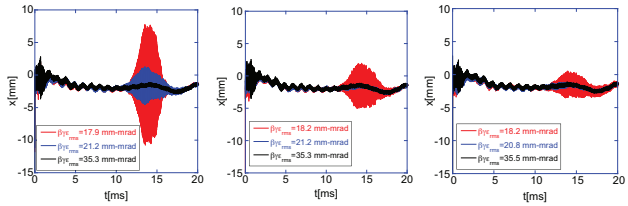

Figure 11: Dependence on transverse emittances with diode units attaching only to No. 8 (left), only to No. 5 (center), and to both Nos. 5 and 8 (right) for a 0.76-MW beam.

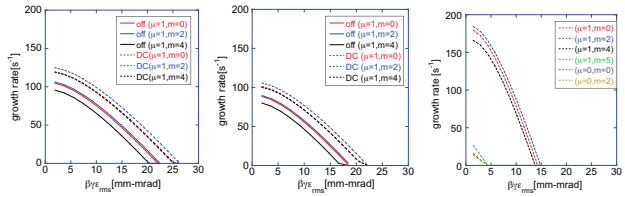

Figure 12: Beam growth rate at 14 ms with diode units attached for 0.76-MW (left/center) and 2-MW beams (right).

Figure 11 shows the dependence of beam growth rate on the emittances under the tracking pattern depicted by the red in the right panel of Fig. 2, where the chromaticity is half-corrected at the injection energy by DC power supply. In the left, center, and right panels, the diode units are attached only to Kicker No. 8, only to Kicker No. 5, and to both Kickers Nos. 5 and 8, respectively. We can clearly identify the kicker position dependence for the effectiveness of the damping effect from the diode unit, as the beam instabilities are enhanced. For comparison, Fig. 12 shows the theoretical results of beam growth rate for different emittances at 14 ms with diode units, where the dashed and solid lines respectively represent the cases that the sextupole magnets are half corrected at the injection energy by DC power supply, and those are turned off at 10 ms. The left and center panels show the cases with the diodes attaching only to No. 8, and to both Nos. 5 and 8 for a 0.76-MW beam, respectively. The

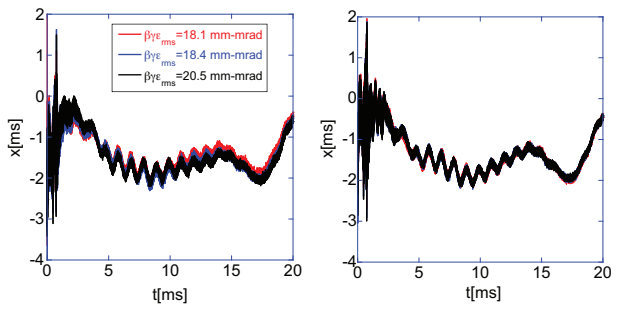

Figure 13: Dependence on tune tracking patterns for a 0.76 MW-beam (left); and beam positions for a 1-MW beam with $\beta_s\gamma_s\epsilon_{rms} = 26$ mm-mrad on the red tracking (right), with diode units attached to Kickers Nos. 2, 4, 5, and 8.

theoretical results match the measurements by red in Figs. 10 and 11, describing the critical emittance beyond which the beam instability occurs for the respective conditions. Furthermore, the results clearly show the universality of the indirect space charge effect, as the emittance dependence on beam instability is identified regardless of whether the diode unit is attached to any set of kickers.

Finally, we consider the case in which diode units are installed on Kicker Nos. 2, 4, 5, and 8, and the chromaticity is half-corrected at the injection energy using a DC power supply. The left panel of Fig. 13 shows the measured horizontal beam positions for a 0.76-MW beam, color-coded according to the tune-tracking patterns shown in the right panel of Fig. 2. The tunability of beam operation is expanded owing to the suppression of beam instability, in contrast to the results in the right panel of Fig. 11, and the tune dependence is eliminated, consistent with the results in Fig. 10.

The right panel shows three successive shots for a 1-MW beam under the tune tracking pattern specified by the red line in the right panel of Fig. 2, with $\beta_s\gamma_s\epsilon_{rms} = 26$ mm-mrad, which is smaller than that in Fig. 3. The 1-MW beam with a smaller emittance is stabilized, even when the chromaticity is half-corrected at the injection energy by a DC power supply, though the measured rms emittance is broadened from 18 mm-mrad due to the space charge effects [11].

The right panel of Fig. 12 shows theoretical results at $Q_x = 6.434$ and 14 ms for a 2-MW beam with diodes installed on four kickers. This measure enlarges the stable region in the emittance plane, suggesting the possibility of achieving a 2-MW beam without transverse feedback.

SUMMARY

The indirect space-charge effect is essential for realizing high-intensity beams [8, 15, 17], enabling the acceleration of smaller-emittance, high-intensity beams without transverse feedback by just reducing the kicker impedance. The newly developed diode unit [11,22] has expanded the parameter window of the RCS tune diagram by suppressing the kicker impedance to realize higher intensity beams [21, 24]. The sustainability of the diode units has been demonstrated through the routine operation of the RCS.

REFERENCES

[1] K. Yamamoto *et al.*, "Design and actual performance of J-PARC 3 GeV rapid cycling synchrotron for high-intensity operation", *J. Nucl. Sci. Technol.*, vol. 59, no. 9, pp. 1174–1205, Feb. 2024. doi:10.1080/00223131.2022.2038301

[2] J-PARC, Japan Proton Accelerator Research Complex, http://j-parc.jp

[3] J-PARC Center, J-PARC Annual Report 2014, 2015, http://j-parc.jp/documents/annual_report/a_report_2014.pdf#zoom=100

[4] P. K. Saha *et al.*, "Direct Observation of the Phase Space Footprint of a Painting Injection in the Rapid Cycling Synchrotron at the Japan Proton Accelerator Research Complex", *Phys. Rev. ST Accel. Beams*, vol. 12, no. 4, p. 040403, 2009. doi:10.1103/PhysRevSTAB.12.040403

[5] A. W. Chao, *Physics of Collective Beam Instabilities in High Energy Accelerators*. New York, NY, USA: Wiley, 1993.

[6] Y. H. Chin, J. Kamiya, Y. Shobuda, K. Takata, and T. Toyama, "Impedance and Beam Instability Issues at J-PARC Rings", in *Proc. HB'08*, Nashville, TN, USA, paper WGA01, pp. 40–44, Aug. 2008. https://accelconf.web.cern.ch/HB2008/papers/wga01.pdf

[7] H. Hahn, "SNS Extraction Kicker System Impedance Estimate", Brookhaven National Laboratory, BNL-105708-2014-TECH; BNL/SNS Technical Note No. 140, 2004. https://technotes.bnl.gov/PDF?publicationId=35111

[8] Y. Shobuda *et al.*, "Theoretical elucidation of space charge effects on the coupled-bunch instability at the 3 GeV rapid cycling synchrotron at the Japan Proton Accelerator Research Complex", *Prog. Theor. Exp. Phys.*, vol. 2017, no. 1, 013G01, 2017. doi:10.1093/ptep/ptw169

[9] J. Kamiya, T. Takayanagi, and M. Watanabe, "Performance of extraction kicker magnet in a rapid cycling synchrotron", *Phys. Rev. ST Accel. Beams*, vol. 12, p. 072401, 2009. doi:10.1103/PhysRevSTAB.12.072401

[10] Y. Shobuda, Y. Irie, T. Toyama, J. Kamiya, and M. Watanabe, "Measurement scheme of kicker impedances via beam-induced voltages of coaxial cables", *Nucl. Instrum. Methods Phys. Res. Sect. A*, vol. 713, p. 52, 2013. doi:10.1016/j.nima.2013.02.037

[11] Y. Shobuda *et al.*, "Demonstration of a kicker impedance reduction scheme with diode stack and resistors by operating the 3-GeV rapid cycling synchrotron of the Japan Proton Accelerator Research Complex", *Phys. Rev. Accel. Beams*, vol. 26, p. 053501, 2023. doi:10.1103/PhysRevAccelBeams.26.053501

[12] Y. Shobuda, P. K. Saha, M. Yamamoto, Y. H. Chin, Y. Irie, and T. Toyama, "The Kicker Impedance and its Effect on the RCS in J-PARC", in *Proc. HB'14*, East Lansing, MI, USA, paper THO2AB02, pp. 369–373, 2014. https://epaper.kek.jp/HB2014/papers/tho2ab02.pdf

[13] F. Sacherer, "Theoretical Aspects of the Behaviour of Beams in Accelerators and Storage Rings", in in *1st International School of Particle Accelerators "Ettore Majorana"*, ed. by M. Hildred, Geneva: CERN, 1977, p. 17, https://cds.cern.ch/record/118362,

[14] S. Meigo *et al.*, "Beam commissioning for neutron and muon facility at J-PARC", *Nucl. Instrum. Methods Phys. Res. Sect. A*, vol. 600, p. 41, 2009. doi:10.1016/j.nima.2008.11.068

[15] P. K. Saha *et al.*, "Simulation, measurement, and mitigation of beam instability caused by the kicker impedance in the 3-GeV rapid cycling synchrotron at the Japan Proton Accelerator Research Complex", *Phys. Rev. Accel. Beams*, vol. 21, p. 024203, 2018. doi:10.1103/PhysRevAccelBeams.21.024203

[16] A. Burov, "Convective instabilities of bunched beams with space charge", *Phys. Rev. Accel. Beams*, vol. 22, p. 034202, 2019. doi:10.1103/PhysRevAccelBeams.22.034202

[17] N. Yoshimura, T. Toyama, and Y. Shobuda, "Space charge effects on the intrabunch motion under large chromaticity at the main ring in the Japan Proton Accelerator Research Complex", *Phys. Rev. Accel. Beams*, vol. 28, p. 034202, 2025. doi:10.1103/yx9r-lhxq

[18] N. Mounet, "DELPHI: An analytic Vlasov solver for impedance-driven modes", CERN, CERN-ACC-SLIDES-2014-0066, 2014. https://cds.cern.ch/record/1954277

[19] N. Mounet, Direct Vlasov solvers, 2020,

[20] Y. Shobuda and K. Yokoya, "Resistive wall impedance and tune shift for a chamber with a finite thickness", *Phys. Rev. E*, vol. 66, p. 056501, 2002. doi:10.1103/PhysRevE.66.056501

[21] S. Igarashi *et al.*, "Accelerator design for 1.3-MW beam power operation of the J-PARC Main Ring", *Prog. Theor. Exp. Phys.*, vol. 2021, no. 3, 033G01, 2021. doi:10.1093/ptep/ptab011

[22] Y. Shobuda *et al.*, "A Kicker Impedance Reduction Scheme with Diode Stack and Resistor at the RCS in J-PARC", in *Proc. HB'23*, Geneva, Switzerland, pp. 162–169, 2023. doi:10.18429/JACoW-HB2023-TUC4I1

[23] Y. Shobuda *et al.*, "Reducing the beam impedance of the kicker at the 3-GeV rapid cycling synchrotron of the Japan Proton Accelerator Research", *Phys. Rev. Accel. Beams*, vol. 21, p. 061003, 2018. doi:10.1103/PhysRevAccelBeams.21.061003

[24] K. Yamamoto *et al.*, "J-PARC linac and RCS – operational status and upgrade plan to 2 MW", *J. Neutron Res.*, vol. 26, p. 59, 2024. doi:10.3233/JNR-240003